APPLICATION OF THE BACKGROUND-ORIENTED SCHLIEREN TECHNIQUE TO VISUALIZE INDOOR AIRFLOWS

Lia Benetas[1,a,*], Maria Hartmann[1,b], Conrad Voelker[1,c]

[1] Bauhaus-Universität Weimar, Department of Building Physics, Coudraystr. 11A, 99423 Weimar, Germany
ORCiD: [a] 0000-0001-8610-0958, [b] 0000-0002-9409-097X, [c] 0000-0002-3687-0177
[*] Corresponding author: lia.benetas@uni-weimar.de

Abstract
This study focuses on further developments and the application of the background-oriented schlieren (BOS) technique to visualize indoor airflows. It is divided into two parts. First, the BOS setup and its specifications are introduced. Since indoor airflows are usually large-scaled and defined by very small density gradients and small velocities, the setup needs to have a high sensitivity, high resolution, and a large field of view. The setup consists of a high resolution (8688 × 5792 pixels) DSLR camera Canon EOS 5DS R, a background structure of random black pixels (edge length 0.22 mm, density 25 %) on white ground, and two flashlights ELINCHROM BRX 500 (each $500\ Ws$ max.) illuminating the background. For image analysis, the cross-correlation-based program PIVview2C is used. Additionally, the sensitivity and possibilities of the developed setup are presented. Using the settings described, it is possible to visualize temperature gradients of $\Delta\Theta < 0.3\ K$ and virtual image shifting of $\Delta y < 0.1$ pixels.
In the second part, the developed BOS setup was used to visualize the spread of breathing air two-dimensionally when playing wind instruments and singing. Here, various brass and woodwind instruments, as well as the human voice, were studied to assess the spreading range of the breathing air when playing different notes, scales, or musical pieces at different pitches, with different dynamics and articulations. Additionally, velocities of the escaping airflows were measured to assess their extent and to validate the BOS evaluations.

Keywords
flow visualization, background-oriented schlieren, sensitivity study, singers, wind instruments

Statements and Declarations
Competing interests: The authors declare that they have no known competing financial interests or personal relationships that could have appeared to influence the work reported in this paper.

Acknowledgments
The authors would like to kindly acknowledge the orchestra director, the wind players, and singers from the *Deutsches Nationaltheater und Staatskapelle Weimar*. We would also like to thank the photography workshop at the Bauhaus-University Weimar for providing their resources. Furthermore, we would like to express our gratitude to the German Research Foundation DFG for funding this project. Their support is highly appreciated.

Funding information
This article is part of a research project funded by the *German Research Foundation DFG* (Grant no. 444059583).

Author contributions
Lia Benetas contributed to the conceptualization, investigation, project administration, and writing – original draft preparation. Maria Hartmann: investigation, writing – review and editing. Conrad Voelker: supervision, writing – review and editing.

1. Introduction

Density gradients in transparent media are based on differences in temperature or pressure and, therefore, cause differences in the refractive index of the fluid, which is described by the Gladstone-Dale relation. The light passing the density difference is then refracted to the extent of the refractive index gradient, which is described by Snell's law. This refraction due to density differences in transparent media can be visualized by background-oriented schlieren (BOS) as an optical, non-invasive technique.

As BOS consists of a rather simple setup to measure non-invasively under various boundary conditions, it is used intensively in numerous fields ranging from large-scale investigations of helicopter rotor blades (e.g., Bauknecht et al. 2015; Gardner et al. 2019; Raffel et al. 2014) to individual adjustments and calibrations to meet the specific requirements (e.g., Cozzi and Goettlich 2019; Hendiger et al. 2021; Rajendran et al. 2019; Vinnichenko et al. 2020; Zhang et al. 2021).

However, in most studies, BOS is used to visualize rather large density gradients. This study aims to explore the possibilities of the BOS technique regarding small temperature gradients. This helps not only to measure weak indoor airflows, but also answers a common question that arises when working with BOS; this optical technique does not visualize airflows but differences in density in transparent media. As soon as the density gradient is below a certain limit, BOS is not able to depict the flow. By measuring the air temperature at different locations as a reference, it was found that the BOS setup is able to visualize temperature gradients of less than $0.3\ K$. This makes the new setup reliable and applicable to visualizing indoor airflows with very small temperature gradients.

The BOS system developed was then applied to visualize the ejected breathing air when playing wind instruments and singing. This study was conducted during the COVID-19 pandemic where especially orchestras and other musicians were forced to stop rehearsing and performing due to the fear of spreading large amounts of infectious breathing air containing pathogens. Additionally, anemometry was used to confirm the spreading distance when playing different instruments.

2. Setup and sensitivity study

The BOS setup used in this study consists of an irregular background pattern (black pixels on white ground, edge length 0.22 mm, $\rho = 25\ \%$), a high resolution full-frame DSLR camera (Canon EOS 5DS R, effective resolution 8688×5792 pixels and lens ZEISS Milvus 2/135, $f = 135\ mm$), and two flashlights (ELINCHROM BRX 500) illuminating the background structure (**Fig. 1**). Here, $\Delta\varepsilon$ describes the deflection angle of each light ray passing the field of view resulting in a virtual displacement Δy (phase shift) on the camera sensor. The distances Z_D between the background pattern and the density gradient, the distance Z_A between the density gradient and the camera, as well as the overall distance between background and lens systems Z_B, and the distance between lens and image plane Z_i can be adjusted appropriately to fit the desired setup and sensitivity.

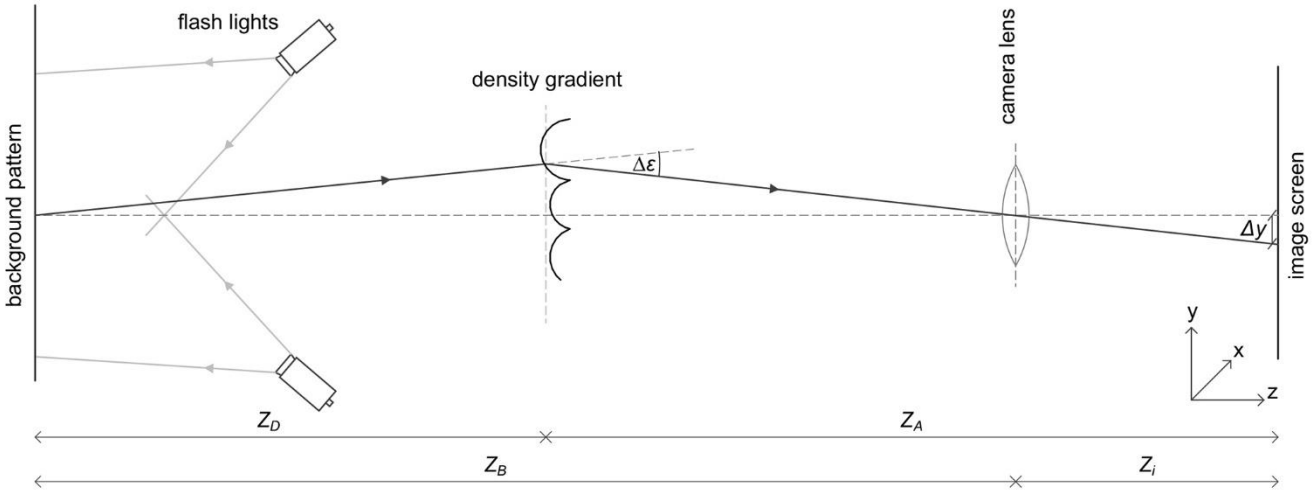

Fig. 1 *Schematic setup of the BOS system at the Department of Building Physics at the Bauhaus-University Weimar*

In this setup, $Z_B = 800\ cm$, $Z_A = Z_D = 400\ cm$, and $Z_i \approx 137\ mm$ at $f = 135\ mm$ were used. Only in section 2.4, the ratio between Z_A/Z_B was varied to assess its impact on the setup's sensitivity.

To visualize the density gradient, a recording of the undisturbed background structure (flow-off) as well as a recording of the density gradient in front of the background (flow-on) are required. Due to the refractive index gradient, each light ray passing the gradient is refracted so that a pixel on the flow-on image appears at a different location compared to the flow-off image. Using cross-correlation algorithms (here: PIVview2C developed by the German Aerospace Center DLR), it is then possible to determine the image shift of each individual pixel, and thus, to visualize the density gradient (Becher et al. 2020a).

In the following sections, the variables of the BOS setup will be discussed to assess their impact on the evaluations, to increase the sensitivity of the system, and further to gather quantitative information from the studies conducted.

2.1. Background structure

Based on the findings in Becher et al. (2020a), a background structure consisting of black pixels with an edge length of $0.22\ mm$ on white ground with a total density of 25% was used for the following studies. Regarding the size of the pixel structure, Raffel (2015) states that the imaging of one background dot on approximately 3-5 pixels of the camera sensor is optimal; 2-3 pixels would increase the sensitivity further but due to diffraction at small apertures and the small pixel pitch of current cameras this hardly can be reached (Raffel 2015). However, in the setup described with an object width $Z_B = 800\ cm$, one background pixel is mathematically displayed on approximately $0.9\ px$ of the camera sensor using the thin lens equation:

$$B = \frac{Z_i \cdot G}{Z_B} \tag{1}$$

with $Z_i \approx 137\ mm$: image width, $Z_B = 8000\ mm$: object width, $G = 0.22\ mm$: object size, B: image size.
When capturing the background at $B \approx 0.9\ px$, the pixel structure appears similar to a noise structure with a lower contrast (**Fig. 2**). The reasons include various inaccuracies as aberrations, diffraction at small apertures, and the small pixel pitch of the used camera, which leads to blurring and image noise. Due to these diffractions and the large distance Z_B between camera and background, the single pixels of the background structure are no longer identifiable in the final image. However, the cross-correlation algorithm used was still able to detect the small displacements when comparing the intensity values of the images.

Fig. 2 *Detail (1 × 2 mm) of the background structure captured at a resolution of 8688 × 5792 pixels and* $Z_B = 800cm$

2.2. Camera settings

Since the camera focuses on the background to allow for capturing the phase shift, a small aperture needs to be chosen in a BOS setup to increase the depth of field and, therefore, to increase the sharp imaging of the density gradient. The depth of field is limited by the near point and the far point and reaches its maximum at the camera's focus point. Due to the depth of field being limited to a certain distance, the density gradient under investigation will appear blurred in the images. Additionally, if the distance between density gradient and focus point increases, the pixel shift Δy increases proportionally to Z_D. By narrowing the aperture's diameter, the depth of field increases slightly as the near point moves further towards the density gradient. The near point g_v for reproduction scales smaller than 1:10 is calculated as follows (Maschke 2004):

$$g_v = \frac{Z_B f^2}{f^2 + ku(Z_B - f)} \tag{2}$$

with $f = 135\ mm$: focal length, u: distraction circle, k: aperture number.
The distraction circle refers to the diameter of an image point that is still detectable and should still appear sharp when the image is taken. The approximation that refers to the perception by the human eye is calculated as follows (Maschke 2004):

$$u = d/1500 \tag{3}$$

with $d \approx 43\ mm$ being the sensor's diagonal. However, it must be taken into consideration that for high image enlargements u must be chosen smaller.
By increasing k stepwise, the distance between density gradient and near point will be reduced from approximately $280\ cm$ at $k = 14$ to $230\ cm$ at $k = 22$ (smallest possible diameter of the aperture). Aperture numbers smaller than $k = 14$ were not considered further due to the insufficient depth of field. However, even when working with such small apertures, the density

gradient will never be imaged in full sharpness. Using an image editing software (Photoshop CC) for post processing, it can be seen that the edges of the object under investigation shot at $k = 20$ and $k = 22$ differ by only one pixel. Therefore, the aperture number k can be kept high to allow the light rays to travel in nearly paraxial space and reduce various aberrations.
Since additional illumination becomes necessary with small apertures, the shutter speed no longer influences the exposure time of the camera when working with flashlights. In this case, the exposure time depends on the guide number of the flashlights. The effective guide number $t_{0.5}$ describes the time interval between the first time when 50% of the maximum flash intensity is reached until it drops to the same value. The variable $t_{0.5}$ can be converted to the absolute guide number $t_{0.1}$ by the factor 3.2. Since the absolute exposure time is of interest, $t_{0.1}$ is better suited as a guide number in these investigations. Regarding the flashlights ELINCHROM BRX 500 at $t_{0.5} = 1/1558\ s$, $t_{0.1} \approx 1/500\ s$ at the highest power level of $500\ Ws$. Due to the flash sync time, which becomes relevant with mechanical shutter as used with the Canon EOS 5DS R, the shutter speed was set to $1/160\ s$.
The illumination time given by the flashlights directly affects the motion blur. Knowing the illumination time and the relative flow velocity (assumption: only vertical flow), the path distance of the air molecules can be calculated and, thus, the motion blur. The proportional path distance in percent at distance Z_A is calculated by:

$$s_{rel} = \frac{s \cdot 100}{b} \quad (4)$$

with s: path distance of an air molecule, b: searched image height at distance Z_A. Furthermore, the image height b depends on the aperture angle α of the camera:

$$b = 2 \cdot (Z_A - f) \cdot \tan(\alpha/2) \quad (5)$$

With an aperture angle of $\alpha = 10.16°$, the image height is $b = 68.7\ cm$. The proportional path distance is projected onto the sensor's height $b' = 24\ mm$. Theoretical calculations according to the described method show that with an illumination time of $1/500\ s$, the vertical pixel shift is less than 1 pixel below flow velocities of $0{,}088\ m/s$.
However, the flashlights were never used at the highest power level. The lower the power level, the shorter the burning time, respectively. There is no proportional relationship between power level and burning time, since the burning time at different power levels depends on several electronic components of the flashlights (e.g., capacitors). Comparatively, the flow velocity can reach $0.177\ m/s$ within an illumination time of $1/1000\ s$ for the same pixel shift. It should be noted that the motion blur increases with increasing flash power level.
During the investigations, the ISO value of the camera was set to 100 to reduce the appearance of noise in the images.

2.3. Illumination

The luminosity can be examined either by evaluating the histograms directly using the camera's software or by using appropriate image editing software. The mean value, which is defined as the arithmetic mean of all grey values in a histogram, is between 0 and 255 and serves as reference. It was found that the optimal mean value for the flow-off image is approximately 170. A lower mean value leads to image noise in the final evaluations. Additionally, lower and higher mean values result in insufficient contrast and, therefore, lower the visibility of the density gradient in the evaluations. The mean value of the flow-on image varies due to the changing size of the object under investigation covering the background pattern. Additional light sources (e.g., ambient light) affect the histogram's mean value negligibly ($\Delta < 1$) due to the small apertures used. Furthermore, to obtain images with the highest possible contrast, it has to be ensured that the tonal values of the histogram are evenly distributed (Gonzalez and Woods 2007).

2.4. Distances within the setup

As already investigated in Becher et al. (2020a), Δy increases with increasing Z_D. Furthermore, varying Z_B while keeping Z_A/Z_B constant has barely an impact on the pixel displacement.
To specify the impact of varying the position of the density gradient within the setup (Z_A/Z_B), the following diagram (Fig. 3) was developed. It shows the pixel shift as a function of Z_A/Z_B depending on the temperature difference. Dashed lines show the distance between the density gradient and the near point depending on the aperture k and the relation Z_A/Z_B.

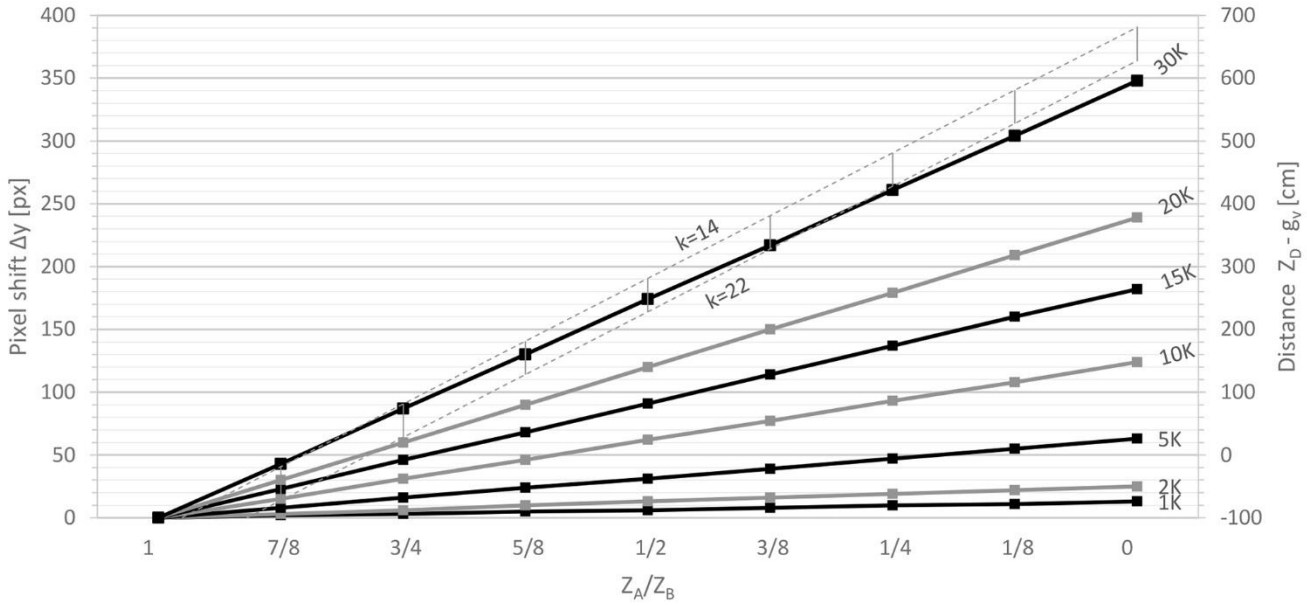

Fig. 3 *Pixel shift Δy as a function of Z_A/Z_B and the depth of field depending on the aperture k: Since Δy hardly varies when varying Z_B, the absolute value of Z_B is irrelevant*

2.5. Minimal displayable temperature gradient

To explore the possibilities of the BOS setup, a controllable ceramic heating resistor (TE Connectivity) was used to induce a nearly two-dimensional convective flow with very little temperature gradients. To verify the temperature gradient, three NTC thermistors with an accuracy of ± 1.5 % and a resolution of $0.01\ K$ were installed to measure the temperature directly at the heating resistor, at $0.7\ cm$ above its surface, and the undisturbed room air temperature outside the thermal plume. The sensors were connected through single strands with small diameters for small measuring errors. In this specific setup, the following parameters were set on the basis of the conclusions from sections 2.1 - 2.4: $k = 22$, shutter speed $1/160\ s$, ISO 100, $Z_B = 800\ cm$, $Z_A = Z_D = 400\ cm$. During the investigations, the camera focused on the structured background. The background was illuminated using two ELINCHROM BRX 500 at a distance of $150\ cm$ to the background. The room air temperature was $\Theta_{room} = 21.8\ °C$. Ventilation systems, heating, and cooling were turned off to avoid any disturbing airflows. This is especially necessary when visualizing small temperature gradients $\Delta T \ll 1K$. For image analysis, PIVview2C was used with the following settings: initial sampling window: $32 \times 32\ px$, final window size $24 \times 24\ px$, step size $12 \times 12\ px$, overlap 50 %, standard (FFT) correlation, sub-pixel image shifting enabled.

As an example, **Fig. 4** shows an evaluation of the convective heat release above the heating resistor (black rectangle) with a temperature $\Theta_r = 27.1°C$ dependent on the voltage. While the temperature difference between the surface of the resistor and the ambient room air is $\Delta\Theta = 5{,}3\ K$, the temperature difference between the convective heat release and the room air at a height of $7mm$ (red line above the resistor) is only $\Delta\Theta = 0.3\ K$. At a height $> 7mm$, the temperature gradient within the thermal plume of the heating resistor is much lower and, therefore, is vaguely visible to the naked eye. Nevertheless, the quantitative image analysis in **Fig. 4** clearly shows the increasing pixel Δy shift due to the convective heat release.

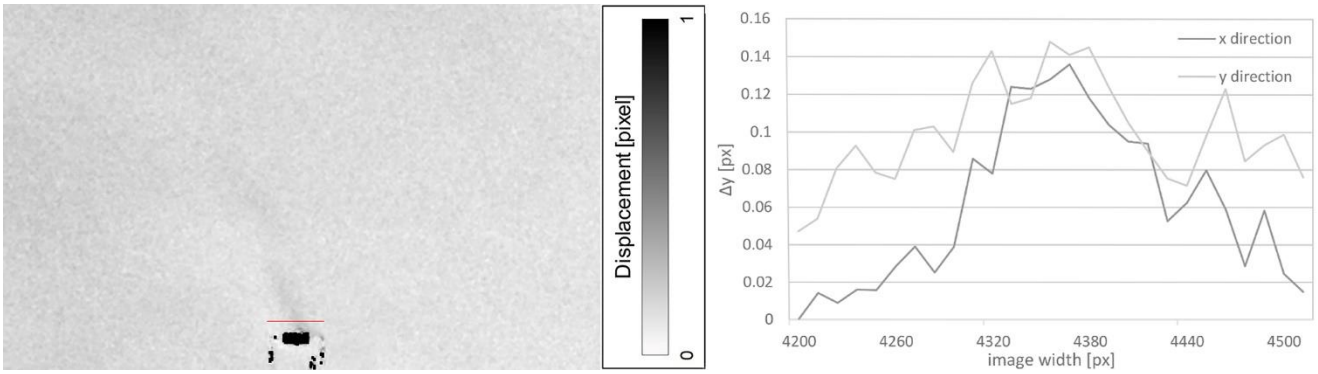

Fig. 4 *Convective heat release above the heating resistor (black rectangle) at $\Delta\Theta = 0{,}3K$ and pixel shift at $h = 0.7\ cm$ ($y = 4428\ px$ image height) (red line) above the resistor*

Using the setup described above, very small temperature gradients of $\Delta\theta = 0.3\ K$ can be visualized. Since the spatial spread of the schlieren is recognizable in the evaluation, it can be assumed that even smaller temperature gradients $\Delta\theta \ll 0.3\ K$ can be displayed with the setup described.

Using PIVview2C for image analysis, it is also possible to analyze the images quantitatively. The one- (**Fig. 5**a) and two-dimensional histograms (**Fig. 5**b) plot the calculated displacement data of the visualization shown in **Fig. 4**, where the mean vectors for each interrogation window are represented by one dot in the two-dimensional histogram. To exclude randomized pixel shifts, it is necessary to mask the object under investigation that induces the density gradient. The horizontal displacement is primarily between $0.05 - 0.1\ px$ ($0.21 - 0.41\ \mu m$), the vertical primarily between $0.05 - 0.15\ px$ ($0.21 - 0.62\ \mu m$). **Fig. 5**c shows the noise of the area outside of the convective flow.

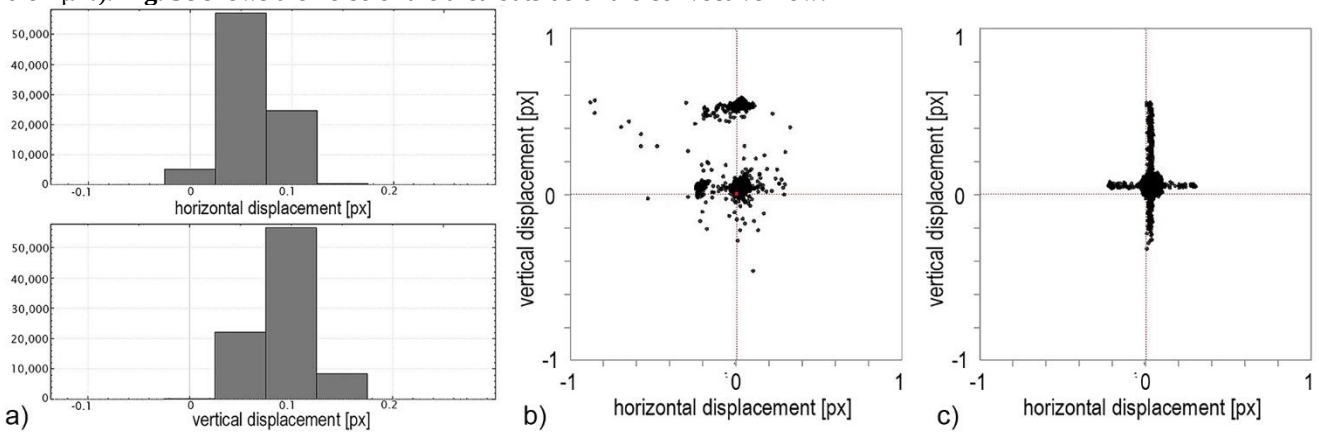

Fig. 5 *One- (a) and two-dimensional histogram (b) of the airflow above the heating resistor, and background noise (c) shown in Fig. 4*

3. Application to indoor airflows

In section 2, it was concluded that the BOS setup is able to visualize temperature gradients $\Delta\theta < 0.3\ K$, which makes it applicable to study indoor airflows, which are defined by very small temperature gradients and small velocities.

In this application, BOS was used to assess the extent of potentially infectious breathing air escaping from wind instruments and singers. Due to the COVID-19 pandemic, orchestras and other musicians were forced to pause rehearsing and performing. Using the BOS technique, recommendations could be given on how far the potentially infectious breathing air containing pathogens could travel and cause direct risk of infection to other occupants. These recommendations and findings have been published previously to help professionals and amateurs assess the direct risk posed by playing wind instruments and singing (Becher et al. 2020b; Becher et al. 2020c; Becher et al. 2021).

In the following work, the evaluations that were collected during the measurements reported in Becher et al. (2021) were used further to assess the virtual image displacement quantitatively. Here, only an excerpt of the reported images in Becher et al. (2021) are shown to validate exemplarily the visualizations using the findings discussed in section 2. The example in **Fig. 6** shows an excerpt of the evaluation from a soprano singer when singing a musical piece.

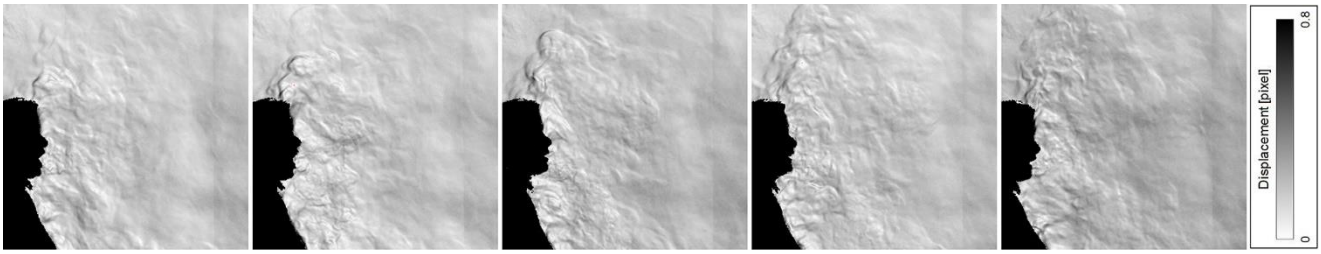

Fig. 6 *Escaping breathing air from the mouth of the soprano singer when singing a musical piece, captured at* $1.5\ fps$

The aim of the study was to analyze the extent of the ejected breathing air. The question that arose during these investigations was whether the evaluations and recommendations are reliable. This is due to BOS only visualizing density gradients as already mentioned earlier. Therefore, the evaluations have to be verified by defining the possibilities of the BOS system to visualize density gradients $\Delta\theta \ll 0.3\ K$ and by using anemometry to define the extent of the ejected airflow (**Fig. 7**).

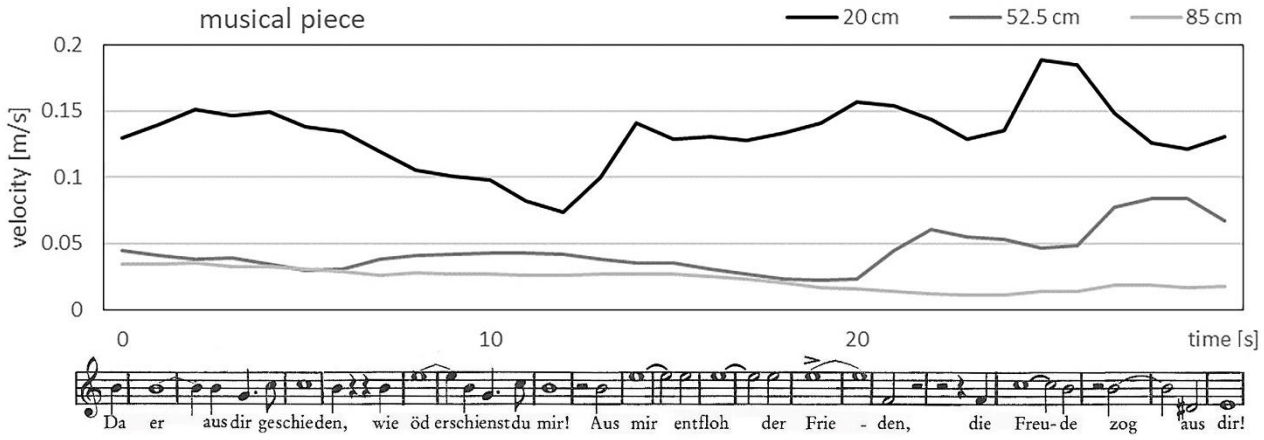

Fig. 7 *Velocities of the ejected airflow from the soprano singer when singing a musical piece at different locations (Becher et al. 2021)*

The anemometry measurements show that there are only very small movements at the farthest sensor at $85\ cm$, which could occur due to the surrounding room air moving slightly. This supports the visualization in **Fig. 8**a, showing the maximal spreading range of the escaping breathing air from the mouth of the soprano singer.

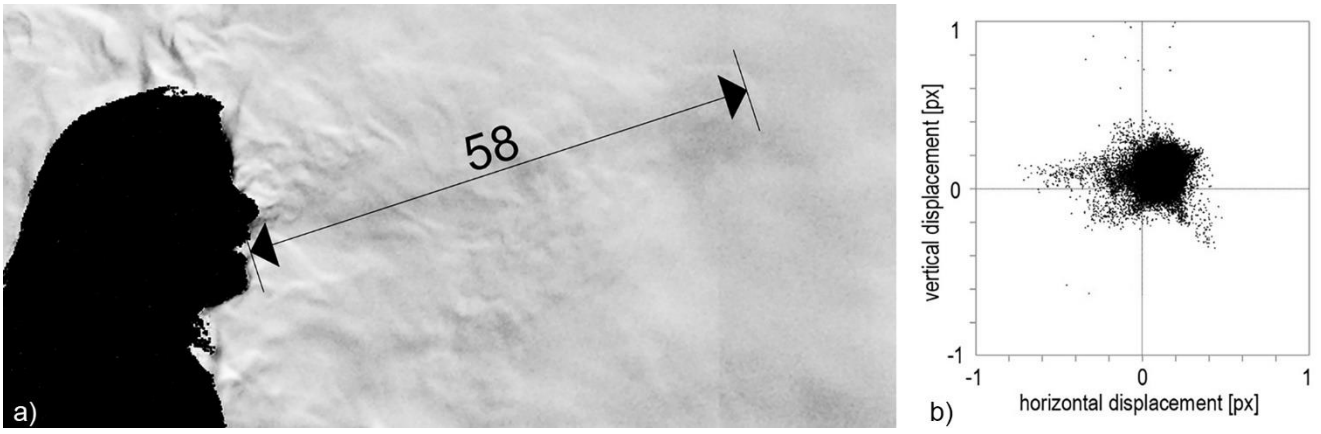

Fig. 8 *Maximal spreading range of the escaping air from the mouth of the soprano singer (a) and two-dimensional histogram of the evaluation (b)*

When evaluating the air ejected by the soprano singer, the horizontal displacement is primarily between $0.1 - 0.2\ px$ ($0.41 - 0.83\ \mu m$), the vertical primarily between $0.05 - 0.15\ px$ ($0.21 - 0.62\ \mu m$) (**Fig. 8**b). Comparing this histogram to **Fig. 5**b where even smaller displacements occur, it can be assumed that the evaluations shown in **Fig. 6** display nearly the full extent of the ejected breathing air. However, specifically regarding the COVID-19 pandemic, only limited conclusions can be drawn regarding the spread of infectious droplets and aerosols as BOS only visualizes density gradients.

For wind instruments, visualizing the breathing air was more difficult compared to the singers due to the air cooling down when going through the bore of the instrument. This applies especially for wind instruments with a long or wide bore (e.g., F tuba, contrabassoon). **Fig. 9** exemplary shows the ejected breathing air when playing the note $Bb6 \approx 1865\ Hz$ on a Bb trumpet.

Detailed information as well as further visualizations of different wind instruments and singers can be found in Becher et al. (2021).

Fig. 9 *Escaping breathing air from the bell of the Bb trumpet when playing the note $Bb6 \approx 1865\ Hz$, captured at $1.5\ fps$*

4. Conclusions

BOS is a rather simple technique to visualize very small density gradients in transparent media. The simple setup and the possibility to adapt the setup easily to any boundary conditions are the main advantages of the BOS system. In this study, the possibilities of the BOS technique were explored to define the smallest detectable density gradient (i.e., temperature gradient). Adapting the different variables adequately, it is possible to visualize temperature gradients $\Delta\theta < 0.3\,K$ with the setup described. When increasing the sensitivity further by decreasing Z_A/Z_B, it will be possible to visualize even smaller gradients $\Delta\theta \ll 0.3\,K$. However, as the camera only focuses on the background, the sharp imaging of the density gradient decreases.
Furthermore, BOS was used successfully to visualize the spread of breathing air when playing wind instruments and singing. Additionally, the evaluations were analyzed further to assess the vertical and horizontal image displacements quantitatively.

5. Limitations

Although it is easy to depict the density gradient in the visualizations shown above, the air could still travel farther than what the visualizations illustrate due to too much air entrainment. Nevertheless, the findings showed that the minimal displayable temperature gradient is $\Delta\theta < 0.3\,K$. However, the BOS method only visualizes density gradients due to differences in temperature or pressure. Therefore, the actual dispersion of the airflow could differ from what can be detected in the visualizations.
The airflow under investigation was captured at $1.5\,fps$, which might be a suitable frame rate for slow convective flows. However, when flow velocities increase, the frame rate has to be adapted to adequately track the direction and the extent of the flow.

References

Bauknecht A, Ewers B, Wolf C, Leopold F, Yin J, Raffel M (2015) Three-dimensional reconstruction of helicopter blade–tip vortices using a multi-camera BOS system. Experiments in Fluids 56:381. https://doi.org/10.1007/s00348-014-1866-6

Becher L, Voelker C, Rodehorst V, Kuhne M (2020a) Background-oriented schlieren technique for two-dimensional visualization of convective indoor air flows. Optics and Lasers in Engineering 134, 106282. https://doi.org/10.1016/j.optlaseng.2020.106282

Becher L, Muehlenberend A, Gena AW, Voelker C (2020b) Einsatz von Filtern zur Reduktion der Ausbreitung der Atemluft beim Spielen von Blasinstrumenten und beim Singen während der COVID-19 Pandemie [Preprint]. https://doi.org/10.13140/RG.2.2.17749.86248

Becher L, Gena AW, Voelker C, Richter B, Spahn C (2020c) Risk assessment of the spread of breathing air from wind instruments and singers during the COVID-19 pandemic. 1st update [Preprint]. https://doi.org/10.13140/RG.2.2.18313.67683/1

Becher L, Gena AW, Alsaad H, Richter B, Spahn C, Voelker C (2021) The spread of breathing air from wind instruments and singers using schlieren techniques. Indoor Air. https://doi.org/10.1111/ina.12869

Cozzi F, Goettlich E (2019) Enhanced Background Oriented Schlieren (EBOS). J. Phys.: Conf. Ser. 1249:12017. https://doi.org/10.1088/1742-6596/1249/1/012017

Gardner AD, Wolf CC, Raffel M (2019) Review of measurement techniques for unsteady helicopter rotor flows. Progress in Aerospace Sciences 111:100566. https://doi.org/10.1016/j.paerosci.2019.100566

Gonzalez RC, Woods RE (2007) Digital Image Processing: Third Edition. Prentice Hall International, Hoboken

Hendiger J, Chludzińska M, Ziętek P (2021) Assessment of the background oriented schlieren application in testing the temperature limit of an axisymmetric ventilation jet. Journal of Building Engineering 35:101964. https://doi.org/10.1016/j.jobe.2020.101964

Maschke T (2004) Digitale Kameratechnik: Technik digitaler Kameras in Theorie und Praxis. Springer Berlin Heidelberg

Raffel M (2015) Background-oriented schlieren (BOS) techniques. Experiments in Fluids 56:132. https://doi.org/10.1007/s00348-015-1927-5

Raffel M, Heineck JT, Schairer E, Leopold F, Kindler K (2014) Background-Oriented Schlieren Imaging for Full-Scale and In-Flight Testing. J Am Helicopter Soc 59:1–9. https://doi.org/10.4050/JAHS.59.012002

Rajendran LK, Bane SPM, Vlachos PP (2019) Dot tracking methodology for background-oriented schlieren (BOS). Exp Fluids 60. https://doi.org/10.1007/s00348-019-2793-3

Vinnichenko NA, Pushtaev AV, Plaksina YY, Uvarov AV (2020) Measurements of liquid surface relief with moon-glade background oriented Schlieren technique. Experimental Thermal and Fluid Science 114:110051. https://doi.org/10.1016/j.expthermflusci.2020.110051

Zhang P, Xu Z, Wang T, Che Z (2021) A method to measure vapor concentration of droplet evaporation based on background oriented Schlieren. International Journal of Heat and Mass Transfer 168:120880. https://doi.org/10.1016/j.ijheatmasstransfer.2020.120880